Applied Catalysis B: Environmental 224 (2018) 125–135

Contents lists available at ScienceDirect

Applied Catalysis B: Environmental

journal homepage: www.elsevier.com/locate/apcatb

Research paper

Chemical CO_2 recycling via dry and bi reforming of methane using Ni-Sn/Al_2O_3 and Ni-Sn/CeO_2-Al_2O_3 catalysts

T. Stroud[a], T.J. Smith[a], E. Le Saché[a,b], J.L. Santos[b], M.A. Centeno[b], H. Arellano-Garcia[a], J.A. Odriozola[b], T.R. Reina[a,*]

[a] Department of Chemical and Process Engineering, Faculty of Engineering and Physical Sciences, University of Surrey, Guildford, GU2 7XH, UK
[b] Departamento de Química Inorgánica, Universidad de Sevilla, Instituto de Ciencias de Materiales de Sevilla Centro mixto US-CSIC, Avda. Américo Vespucio 49, 41092 Seville, Spain

ARTICLE INFO

Keywords:
CO_2 utilisation
Dry reforming
Bi-reforming
Ni-Sn catalysts
Syngas

ABSTRACT

Carbon formation and sintering remain the main culprits regarding catalyst deactivation in the dry and bi-reforming of methane reactions (DRM and BRM, respectively). Nickel based catalysts (10 wt.%) supported on alumina (Al_2O_3) have shown no exception in this study, but can be improved by the addition of tin and ceria. The effect of two different Sn loadings on this base have been examined for the DRM reaction over 20 h, before selecting the most appropriate Sn/Ni ratio and promoting the alumina base with 20 wt.% of CeO_2. This catalyst then underwent activity measurements over a range of temperatures and space velocities, before undergoing experimentation in BRM. It not only showed good levels of conversions for DRM, but exhibited stable conversions towards BRM, reaching an equilibrium H_2/CO product ratio in the process. In fact, this work reveals how multicomponent Ni catalysts can be effectively utilised to produce flexible syngas streams from CO_2/CH_4 mixtures as an efficient route for CO_2 utilisation.

1. Introduction

Finding solutions to reducing the amount of carbon dioxide being emitted to the atmosphere remains of great importance. A common approach for mitigating the associated global climate change is to capture CO_2 and deposit it in saline aquifers [1]. Alternatively, CO_2 can be converted into valuable products via catalytic reactions [2]. Among the different products, syngas is one of the most preferred since it represents a major intermediary for several industries, such as the production of methanol and many other commodity chemicals. The most widely practiced production route of syngas is steam reforming (SRM) [3]:

$$\begin{aligned} &CH_4 + H_2O \rightleftharpoons CO + 3H_2 \\ \text{SRM:}\quad &\Delta H_{298K} = +206\ \text{kJ/mol} \\ &\Delta G_{298K=} + 142\ \text{kJ/mol} \end{aligned} \tag{1}$$

However, this process requires high temperatures (typically above 800–900 °C) and large amounts of steam to proceed [3]. Alternatively, CO_2 can be used to produce syngas in conjunction with methane by the following routes:

$$\begin{aligned} &CH_4 + CO_2 \rightleftharpoons 2CO + 2H_2 \\ \text{DRM:}\quad &\Delta H_{298K} = +247\ \text{kJ/mol} \\ &\Delta G_{298K=} + 170\ \text{kJ/mol} \end{aligned} \tag{2}$$

$$\begin{aligned} &3CH_4 + CO_2 + 2H_2O \rightleftharpoons 4CO + 8H_2 \\ \text{BRM:}\quad &\Delta H_{298K} = +220\ \text{kJ/mol} \\ &\Delta G_{298K=} + 151\ \text{kJ/mol} \end{aligned} \tag{3}$$

$$\begin{aligned} &3CH_4 + CO_2 + O_2 \rightleftharpoons 4CO + 6H_2 \\ \text{ORM:}\quad &\Delta H_{298K} = +58\ \text{kJ/mol} \\ &\Delta G_{298K=} - 1\ \text{kJ/mol} \end{aligned} \tag{4}$$

Whilst oxy-CO_2 reforming (ORM, Eq. (4)) is arguably the most attractive (being autothermic), safety issues associated with the use of oxygen limit the attractiveness to industry [3] and hence will not be considered further in this work.

For the bi-reforming of methane (BRM, Eq. (3)), its main advantage over dry reforming of methane (DRM, Eq. (2)) is the stoichiometric H_2/CO ratio of 2. This is a more favourable syngas composition for most downstream operations, such as conversion to liquid fuels via Fischer-Tropsch synthesis (FTS) [4]. This ratio can also be easily varied by adjusting the inlet composition of the feed gases with respect to CO_2

* Corresponding author.
E-mail address: t.ramirezreina@surrey.ac.uk (T.R. Reina).

http://dx.doi.org/10.1016/j.apcatb.2017.10.047
Received 27 July 2017; Received in revised form 21 September 2017; Accepted 18 October 2017
Available online 19 October 2017

and H_2O [5]. Furthermore, the presence of steam simultaneously drives SRM (Eq. (1)), which gives rise to the selectivity for H_2 and CO both being 100% (with respect to methane), as CO_2 and CH_4 net formation is zero whilst controlling the H_2/CO ratio [6].

Conditions used for reforming also favour other side reactions, such as the reverse water gas shift (RWGS), the Boudouard reaction and C oxidation/reduction processes (Eqs. (5)–(10)), which can affect the distribution of products as well as the catalytic performance.

RWGS: $CO_2 + H_2 \rightleftharpoons CO + H_2O$ (5)

Boudouard: $2CO \rightleftharpoons CO_2 + C$ (6)

CH_4 decomposition $CH_4 \rightleftharpoons C + 2H_2$ (7)

CO reduction: $CO + H_2 \rightleftharpoons C + H_2O$ (8)

C oxidation: $C + ½O_2 \rightleftharpoons CO$ (9)

C oxidation: $C + O_2 \rightleftharpoons CO_2$ (10)

One of the major challenges in hydrocarbon reforming is to avoid catalyst deactivation via carbon deposition (Eqs. (6)–(8)) on the surface, which can cover active sites [7]. Hence, a suitable catalyst for these reactions should be resistant to carbon formation, which may be achieved by enhancing the oxidation reactions (Eqs. (9) and (10)) [8]. BRM has also the added benefit of being able to gasify carbon via the reverse of Eq. (8), and thus resulting in improved catalytic activity [9].

Among the wide variety of reforming catalysts available in literature, nickel based materials have shown good activity towards both DRM and BRM, whilst remaining the best option in terms of manufacturing costs [8,10,11]. Additionally, an alumina (Al_2O_3) support is effective at dispersing the Ni particles due to having a large surface area whilst remaining thermally stable under reforming conditions [4]. However, the inherent acidity of alumina promotes coking and catalyst sintering, the second most prevalent factor for catalyst deactivation [8,12].

The addition of promoters can help to mitigate both carbon deposition and sintering leading to highly efficient materials for reforming reactions [13]. In this regard, ceria (CeO_2) has been extensively studied and shown to greatly improve the performance of Ni based catalysts; particularly those supported on Al_2O_3. Indeed, CeO_2-Al_2O_3 combinations are excellent supports for reforming reactions [10]. This is due to a lower acidity in comparison to bare alumina and the great oxygen storage capacity (OSC) of cerium oxide. The redox properties of ceria facilitate the oxidation of carbon deposits expanding the lifetime of the catalysts [14,15]. Further studies have also revealed that ceria modifies the metal-support interactions, increasing the active phase dispersion and improving the stability of alumina at high temperatures [16].

Together with support modifications, the active phase can also be promoted with the addition of a second metal. Indeed, bimetallic systems typically exhibit superior performance (higher catalytic activity and enhanced carbon resistance) compared to their individual counterparts. This fact is due to multiple effects arising from the bimetallic interaction: (i) a change in the number of active sites (cooperative effects); (ii) the sacrificial role played by one of the species forming the bimetallic system, thus leaving the second metal free and available; and (iii) an electronic effect coming from the metal–metal interactions resulting in less sensitive materials toward carbon poisoning [10]. Within the bimetallic combinations, Ni-Sn materials have proven to be of interest towards reforming reactions [17]. However, there remains some controversy over the affect this has, with some authors stating a positive effect [18–22] and others a negative [23–25]. Tin has a similar electronic structure to carbon, which favours the interaction of Sn p orbitals with Ni 3d electrons, thereby reducing the chance of nickel carbide formation as a coke precursor [26]. Additionally, Ni dispersion over catalyst surfaces has been shown to increase in the presence of Tin [27]. This is an important factor for sintering reduction, and therefore, improving long term catalytic performance.

In this scenario, the aim of this work is to apply advanced Ni-Sn/Al_2O_3 and Ni-Sn/CeO_2-Al_2O_3 catalysts for the chemical recycling of CO_2 via dry and bi-reforming of methane. A deep analysis of the dry reforming reaction conditions (as well as a dry/bi-reforming comparison) opens a fruitful discussion regarding catalyst structure/composition, and the observed performance reveals some key aspects to maximise the catalytic activity and the selectivity towards syngas.

2. Experimental

2.1. Catalyst preparation

The cerium promoted support was synthesized by impregnation of $Ce(NO_3)_2{\cdot}H_2O$ (Sigma-Aldrich) on γ-Alumina powder (Sasol) in order to obtain a 20 wt% of CeO_2. This support, named henceforth as “Ce-Al”, was calcined at 800 °C for 8 h.

All catalysts were prepared by sequential impregnation, where the support was first impregnated with $Ni(NO_3)_2{\cdot}6H_2O$ (Sigma-Aldrich) diluted in acetone, evaporated at reduced pressure in a rotavapor, dried overnight at 80 °C and calcined at 800 °C for 4 h. Afterwards, the solids were impregnated in a similar way with $SnCl_2$ (Sigma-Aldrich) and calcined at 800 °C for 4 h. In all cases the NiO content is calculated to be 10 wt.%. The Sn promoted catalysts were prepared to present Sn/Ni molar ratios of 0.02 and 0.04. These ratios were chosen based on previous works [27].

For the sake of simplicity, all samples will be referred to by only the active components. Ni/Al refers to a catalyst composed of 10 wt.% NiO dispersed on Al_2O_3; $Sn_{0.02}$Ni/Al and $Sn_{0.04}$Ni/Al are 0.02 and 0.04 mol of Sn respectively for every mole of 10 wt.% NiO on an Al_2O_3 base; and $Sn_{0.02}$Ni/Ce-Al is a Sn/Ni molar ratio of 0.02 on a CeO_2-Al_2O_3 support.

2.2. Catalyst characterisation

N_2-adsorption-desorption measurements were performed in a Micrometrics TriStar II 3020 unit at liquid nitrogen temperature. Before the analysis, the samples were degassed at 250 °C for 2 h in vacuum. The Brunauer-Emmett-Teller (BET) equation was applied to the results to calculate surface area, whilst pore-size distributions were determined using the Barett–Joyner–Halenda (BJH) method.

H_2-Temperature Programmed Reduction (H_2-TPR) analysis was carried out in a conventional U-shaped quartz reactor connected to a TCD detector, utilising a 50 ml/min flow of 5% H_2 in an Ar atmosphere (Air Liquide). 50 mg of catalyst was heated from room temperature to 900 °C at a rate of 10 °C/min. A mixture of ethanol and liquid nitrogen was used as cold trap to retain any water produced during the procedure.

X-ray diffraction (XRD) analysis was conducted on fresh and used catalysts using an X’Pert Pro PANalytical instrument. The 2θ angle was increased by 0.05° every 160 s over a range of 10–90°. Diffraction patterns were recorded at 40 mA and 45 kV, using Cu Kα radiation (λ = 0.154 nm).

Scanning electron microscope (SEM) imagery was carried out on a JEOL 5400 equipped with an Energy Dispersive X-ray Spectroscope (EDS) analyser (Oxford Link).

Raman analysis was performed in a Horiba Jobin Yvon dispersive microscope (HR800) with a confocal pinhole of 1,000 µm, a laser spot diameter of 0.72 µm, and a spatial resolution of 360 nm. A diffraction grating of 600 grooves per mm, CCD detector, a green laser with a wavelength of 532.14 nm (maximum power 20 mW), and a 50x objective were also used.

Temperature programmed oxidation (TPO) was conducted in a U-shaped quartz reactor coupled to a PFEIFFER Vacuum PrismaPlus mass spectrometer. Samples were heated up to 900 °C at a rate of 10 °C/min in a flow of 50 ml/min (5% O_2, 95% He)

2.3. Catalytic activity

The dry reforming of methane reaction was carried out in a tubular quartz reactor (10 mm ID) at atmospheric pressure, supporting the catalyst on a bed of quartz wool. CO_2, CH_4, CO and H_2 content were monitored using an on-line gas analyser (ABB AO2020), equipped with both IR and TCD detectors. All the samples were pre-treated in situ by flowing 20% H_2/N_2 for 1 h at 800 °C.

Reactions were operated at temperatures ranging from 600 to 800 °C, using a constant reactant flow of 100 ml/min ($CH_4/CO_2/N_2$: 1/1/6). The mass of catalyst was varied from 50 to 200 mg in order to achieve Weight Hourly Space Velocities (WHSVs) from 30, 000 to 120, 000 ml/(g-cat h). Conversions (X_i) and yields (Y_i) of the different reactants and products were calculated as follows:

$$X_{CH_4}(\%) = 100*\frac{[CH_4]_{In} - [CH_4]_{Out}}{[CH_4]_{In}} \quad (11)$$

$$X_{CO_2}(\%) = 100*\frac{[CO_2]_{In} - [CO_2]_{Out}}{[CO_2]_{Out}} \quad (12)$$

$$Y_{H_2}(\%) = 100*\frac{[H_2]_{Out}}{2[CH_4]_{In}} \quad (13)$$

$$Y_{CO}(\%) = 100*\frac{[CO]_{Out}}{[CH_4]_{In} + [CO_2]_{In}} \quad (14)$$

The bi-reforming of methane reaction was performed in a computerized commercial Microactivity Reference catalytic reactor (PID Eng & Tech), employing a tubular quartz reactor with a 9 mm internal diameter. Gas products were analysed on line using a MicroGC (Varian 4900) equipped with Porapak Q and MS-5A columns. Prior to reaction, the catalyst was reduced for 1 h at 800 °C in 60 ml/min H_2 (10%, v/v in N_2). The gas composition was set to $CH_4/CO_2/H_2O/N_2$: 1/1/1/1 to achieve a WHSV of 60,000 ml/(g-cat h).

2.4. Thermodynamic simulation

ChemStations' ChemCad software package was used to observe the thermodynamic limits of both DRM and BRM reactions over a range of temperatures. The Soave-Redlich-Kwong equation of state was used in a Gibbs reactor. Material flows into the reactor are identical to those intended to be used for experimentation.

3. Results and discussion

3.1. Textural properties

All the samples are mesoporous materials with specific surface area and pore volume governed by the primary support (γ-Al_2O_3). Results obtained from BET analysis (Table 1) show that the addition of Sn barely affects the textural properties of the reference Ni/Al. In contrast, cerium drastically reduces both surface area and pore volume. Indeed, the changes on pores size indicate that CeO_2 nanoparticles may be partially covering the pores of the alumina support, explaining the reduction of surface area and pore volume in good agreement with previous observations in literature [8,20].

Table 1
Textural properties of catalysts, as determined by BET analysis.

Sample	S_{Bet} (m^2/g)	V_{Pore} (cm^3/g)	D_{Pore} (nm)
Ni/Al	164	0.42	10.1
Sn0.02 Ni/Al	173	0.42	9.8
Sn0.04 Ni/Al	172	0.42	9.8
Sn0.02 Ni/Ce-Al	120	0.29	9.6

3.2. XRD

XRD on fresh samples (Fig. 1) shows an absence of metallic nickel (Ni°) and NiO peaks, of which there are two main possible explanations. One is that the Ni was effectively dispersed, resulting in particles smaller than the resolution limit of the XRD equipment (typically ~4 nm). The second possible explanation is that Ni is arranged in the form of aluminate spinel ($NiAl_2O_4$), which can reportedly form via the reaction between NiO and Al_2O_3 under the high calcination temperature (800 °C) used during catalyst preparation [12]. The detection of spinel crystalline peaks coincides with the gamma phase planes (4 4 0), (4 0 0) and (3 1 1) of alumina (JCPDS# 00-048-0367) at 66.79°, 45.76°, and 37.58° respectively. However as previously reported, a Ni loading of approximately 33 wt.% is required for a full transformation to aluminate spinel [28]. Therefore given that the catalysts are 10 wt.% Ni loaded, the most likely situation is that of $NiAl_2O_4$ coexisting with γ-Al_2O_3.

For the ceria containing sample, typical diffraction peaks of the CeO_2 fluorite cubic cell (JCPDS# 00-004-0593) at 28°, 33°, 48°, and 56° were detected (Fig. 1d). The addition of Sn had minor effects to the textural properties and also the crystalline structure of the samples. The most likely phase of Sn to be detected would be that of Ni_3Sn [20], but this is only seen when larger quantities of Sn are added (Sn/Ni > 0.4) [27]. Similarly, Pastor-Pérez et al. [20] found an absence of this phase when coupled to CeO_2, suggesting the formation of this complex only occurs when Ni-support interactions are weak.

Relevant information is extracted from the X-Ray diffraction patterns of the activated samples (reduced in hydrogen) and the spent catalysts (Fig. 1) after catalytic screening. Indeed, Fig. 1 reveals the presence of metallic Ni particles (JCPDS# 45-1027) which are assumed to be the active species in the reforming reaction. Furthermore, the calculated particle size of the Ni cluster using Scherrer equation is ca. 20–23 nm for all the samples. This is very similar to the particle size after reaction, which lies between 20–25 nm; indicating a minor influence of active phase sintering in these catalysts. In addition, the spent samples present typical diffraction peaks of carbon at around 25°, indicating the formation of carbonaceous species with a certain degree of crystallinity during the reaction.

3.3. Reducibility: H_2-TPR

Fig. 2 shows the H_2-TPR profiles for the fresh catalysts with the main peak at around 760 °C on all samples being attributed to the reduction of strong bonding between NiO and the alumina support [27]. Indeed, such a high temperature for Ni reduction indicates the presence of $NiAl_2O_4$ spinel in good agreement with the XRD data.

The addition of Sn does not remarkably affect the TPR profiles. A shift of the main reduction peak towards lower temperatures was observed for the sample with the highest Sn loading, indicating that Sn somehow improves the overall reducibility. As for the ceria doped sample, some major dissimilarities were found. More specifically an additional process appears at around 850 °C, which corresponds to the reduction of the CeO_2 species. Due to the high temperature needed for this reduction, this process is likely related to the reduction of bulk ceria species [20]. Also a smooth reduction event takes place between 200 and 450 °C which signifies a certain degree of ceria surface reduction [20]. In fact, this profile matches well with that of the CeO_2-Al_2O_3 support included for sake of comparison in which the ceria bulk reduction at high temperatures is evident along with a broad reduction process taking place between 280 and 700 °C associated to ceria surface reduction. Both just mentioned processes are shifted towards lower temperatures when Ni is added indicating that Ni facilitates CeO_2 reduction and also evidencing a close Ni-CeO_2 interaction.

Overall it can be inferred from the TPR that Sn appears to help the reducibility of the samples, especially for the highest Sn-loaded material. Importantly, the presence of ceria more remarkably affects the

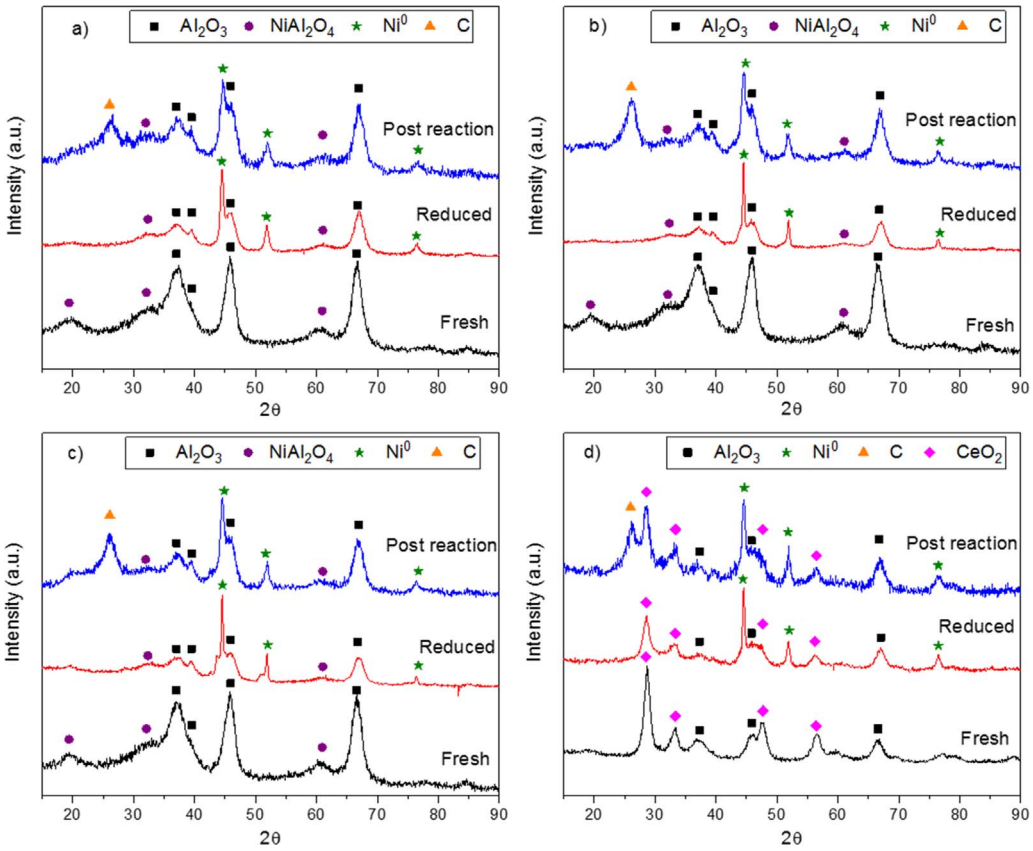

Fig. 1. XRD patterns of each catalyst fresh, reduced and after 20 h of reaction: (a) Ni/Al; (b) $Sn_{0.02}Ni/Al$; (c) $Sn_{0.04}Ni/Al$; (d) $Sn_{0.02}Ni/Ce\text{-}Al$.

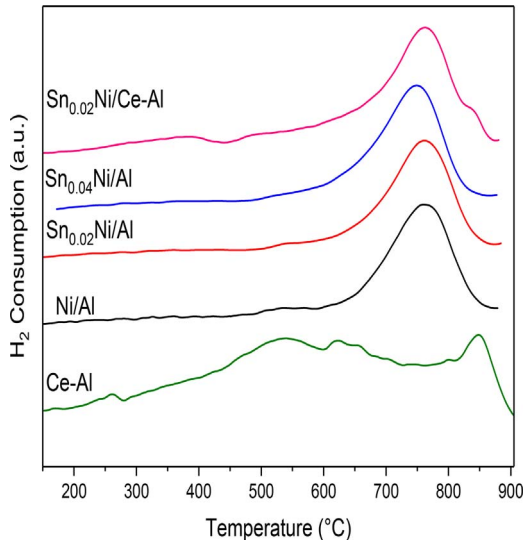

Fig. 2. H_2-TPR profiles of each catalyst.

redox properties of the catalysts, introducing oxygen mobility and altering Ni-support interactions.

3.4. Thermodynamics

By comparing the equilibrium plots of DRM (Fig. 3a) and BRM (Fig. 3b), the benefits of the BRM reaction become prevalent. Carbon formation is reduced at all temperatures due to increased gasification (Eq. (8)) dropping to virtually nil at 700 °C. A greater quantity of CO and H_2 is also produced for lesser quantities of CH_4 and CO_2 at the inlet when compared with DRM, whilst also exhibiting a larger and therefore more favourable H_2/CO ratio.

For DRM, a catalyst operating at 700 °C will have some benefit of reduced carbon formation, but still have the potential to reach an acceptable H_2/CO ratio (1.24) and good conversions. CO_2 conversion for BRM is a more complex matter, as it increases for temperatures up to 550 °C. Hence, a temperature of 700 °C is also preferable as the conversion is improved and an H_2/CO ratio of 1.64 is achievable. In view of these results an interesting comparison between DRM and BRM is described in the following sections.

3.5. Catalyst screening in DRM

All 4 synthesised catalysts underwent DRM reaction at 700 °C for over 20 h of continuous on-stream operation (Fig. 4). As expected, the performance of the Ni/Al reference material deteriorates greatly for all measured aspects. This is credited to the formation of carbon species blocking active sites, partly driven by the previously mentioned acidic nature of alumina [12]. This is evidenced by the SEM imagery (Fig. 5Ic), where the carbon can clearly be seen to be overlaying the surface. Indeed, this type of filamentous carbon formation on Ni is well established and researched [29].

Adapting on work by Baker et al. [30,31], the mechanism can be described by three steps. Carbon that is present in the gas phase (CH_4 and CO_2) disassociates into elemental carbon upon adsorbing to the catalyst surface. Following this, the carbon diffuses through the metallic particles and finally precipitates out in the metal-support interface forming a filament [30,31].

Of the two reactants, methane is said to be the most difficult to activate and therefore methane activation is the rate determining step and the primary means of carbon deposition (Eq. (7)) [32]. This explains why methane conversions are lower than those of CO_2 for all the catalysts. The reference Ni/Al catalyst performed the worst among the studied materials and showed the greatest level of deactivation across the board.

Very interestingly, the addition of Sn clearly improves catalytic

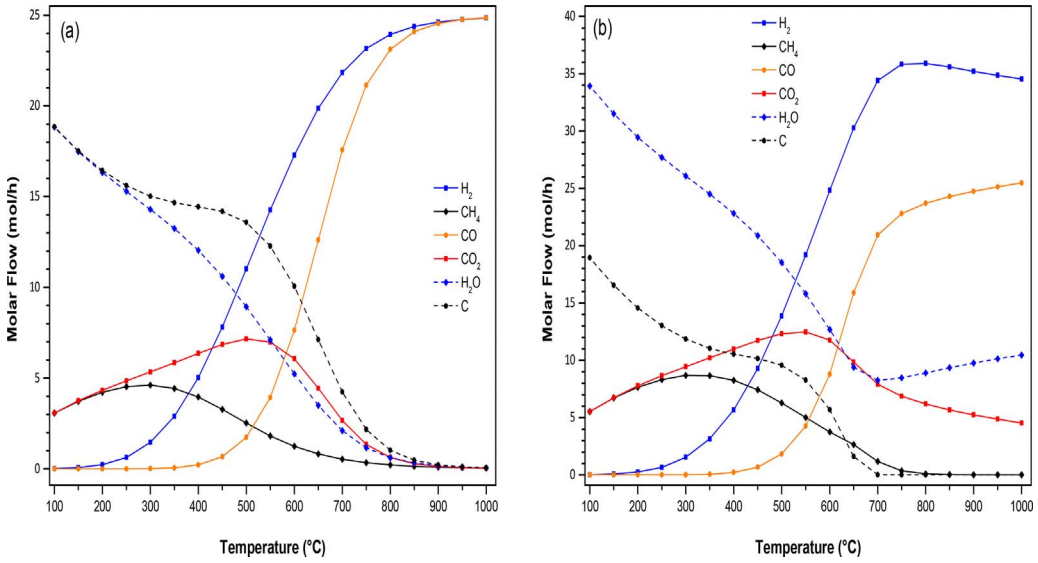

Fig. 3. Equilibrium plots over a temperature range as generated by ChemCad for: (a) DRM ($CH_4/CO_2/N_2$ = 12.5/12.5/75 mol/h); (b) BRM ($CH_4/CO_2/H_2O/N_2$ = all set to 15 mol/h).

performance. The Sn doped samples do in fact perform worse even than Ni/Al for the first 8 h of methane conversion (Fig. 4a), with the lesser 0.02 doped sample performing worst. However over time, this lesser doped sample performs best with a marked improvement over the reference Ni/Al. In other words, the Sn doped samples reached a higher steady sate conversion, indicating its suitability as promoter. The observed improvement is attributed to the greater tolerance to carbon deposition of the bimetallic Ni-Sn catalysts.

Therefore it may be surprising that the slightly greater 0.04 Sn sample performs worse over time. However, this can been attributed to the fact that too great an amount of Sn effectively smothers active sites, preventing access by the reactants and thereby reducing activity in both the long and short term [27]. Hence a trade-off of activity/stability needs to be established, and lower Sn loadings are apparently more advantageous in this sense. Based on this outcome, a Ni/Sn molar ratio of 0.02 was selected for the promotion of Ni/Ce-Al.

In principle, the aforementioned dispersive effects of both CeO_2 and Sn promotion should be combined to efficiently disperse the Ni and drastically reduce sintering. For CH_4 conversion, $Sn_{0.02}$Ni/Ce-Al shows an initially promising start but eventually follows the same trend as the Sn_xNi/Al based catalysts after 10 h, ending at around a 20% conversion. Regarding CO_2 conversion however, $Sn_{0.02}$Ni/Ce-Al (Fig. 4b) outperforms the other catalysts throughout.

Whilst improving dispersion and oxidising carbon, CeO_2 has previously been shown to catalyse the RWGS reaction (Eq. (5)) [33]. This contributes to the higher CO_2 conversion and the comparable H_2/CO

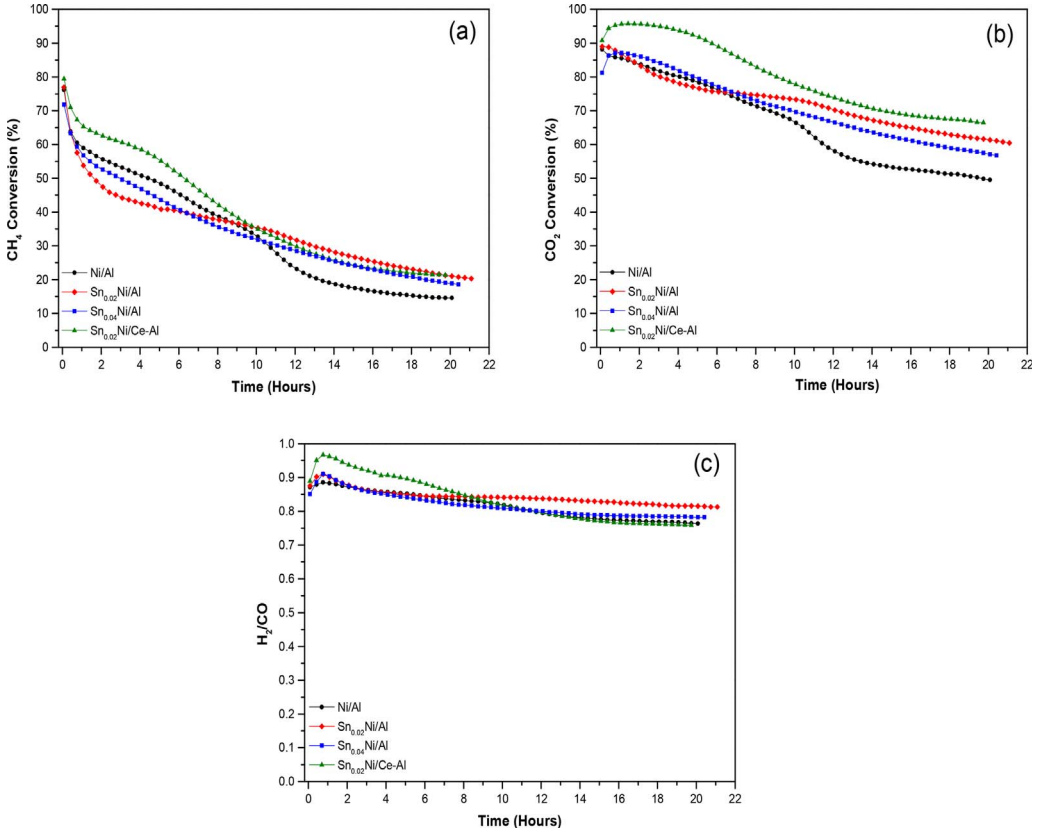

Fig. 4. DRM of all catalyst at 700 °C, a WHSV of 60, 000 ml/(g-cat h) and a CH_4/CO_2 ratio of 1: (a) Methane Conversion; (b) CO_2 Conversion; (c) H_2/CO ratio.

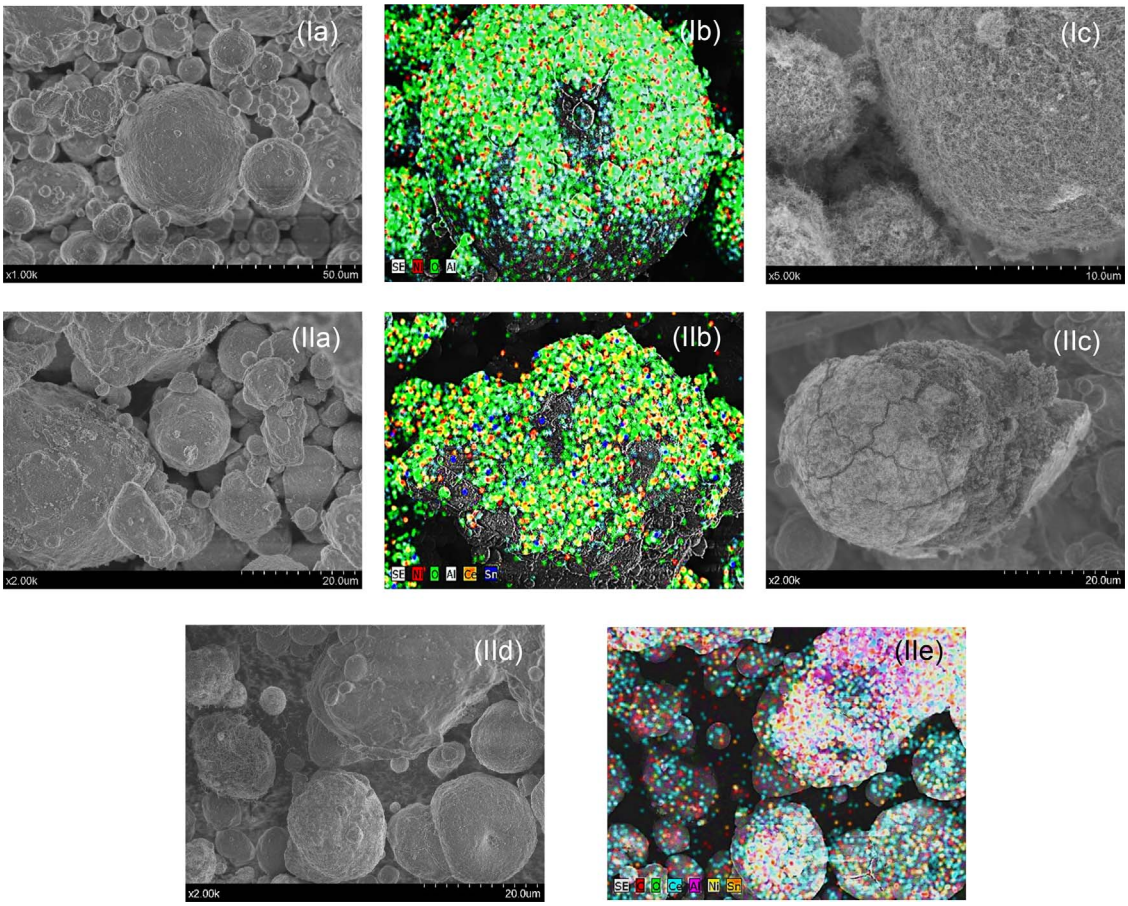

Fig. 5. SEM imagery of catalysts: (I) Ni/Al; (II) $Sn_{0.02}$Ni/Ce-Al; where (a) non-reduced fresh; (b) non-reduced fresh mapping; (c) post reaction; (d) post reaction for mapping; (e) carbon mapping of post reaction based on (d).

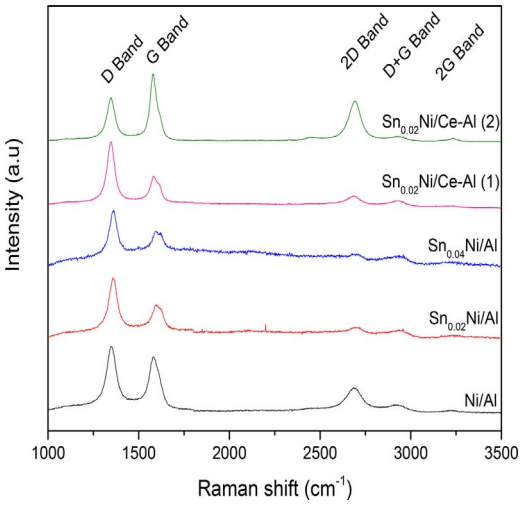

Fig. 6. Raman spectra for all catalysts performed post reaction.

ratio (Fig. 4c) for non-ceria doped samples, as the reaction increases the abundance of CO via CO_2 uptake.

3.6. Study of carbonaceous deposits

3.6.1. SEM

As evidenced by SEM (Fig. 5IId), Ni is well dispersed on the surface in the fresh catalysts and remains as such after 20 h of reaction. Also, as shown in the XRD patterns for post DRM reaction samples, Ni becomes metallic and some means of sintering can be intended (Fig. 1 see comparison fresh/spent); although the activity results (Fig. 4) imply this is reduced through the addition of Sn. It has been suggested that during reduction, a Ni-Sn alloy forms through the diffusion of Sn into Ni [34]. Like fresh samples, there is no evidence of this alloy in the XRD, but it remains possible it is being masked by the presence of the Al phases. For example, Ni_3Sn peaks are expected at 31° and 45° [20] but these also respectively correspond to $NiAl_2O_4$ and metallic Ni peaks, making it difficult to confirm whether Ni_3Sn exists post reaction. As mentioned previously though, a larger amount of Sn may be required for this phase to be unequivocally formed.

It is also clear from the imagery that the morphology of the carbon deposits varies. Fig. 5IIc appears to show a heavy covering of crystalline carbon, with little in the way of filamentous carbon, which is predominantly seen on the Ni/Al surface (Fig. 5Ic). Harder, more crystalline carbon (e.g. graphite) is harder to oxidise, and therefore, is less favourable than softer, more amorphous forms of carbon [7]. For the multicomponent catalysts $Sn_{0.02}$Ni/Ce-Al, the presence of carbon species after DRM was also evidenced. However, the SEM images revealed a poorer degree of crystallinity of these carbon species in comparison to those formed over the Ni/Al catalysts, and thus, pointing out the beneficial effect of CeO_2 and Sn as promoters to mitigates coking.

3.6.2. Raman

Further information regarding the structure of carbonaceous deposits was extracted from the Raman study. The Raman spectra (Fig. 6) confirms that different forms of carbon are present, corroborating the information from SEM. Peaks at 1, 350 (D-band) and 1, 585 cm^{-1} (G-band) are typically ascribed to sp^2–bonded carbon species and assigned to phonons of A_{1g} and E_{2g} symmetry respectively [35]. The D-band

indicates the density of defects in graphitic materials while the G-band corresponds to the tangential vibrations of C−C bonds of the graphitic carbon structures. Thus the relative intensity of these peaks can express the graphitization of carbon materials. The lower the I_D/I_G value is, the higher is the degree of graphitization. Herein the estimated values for Ni/Al, $Sn_{0.02}$Ni/Al, $Sn_{0.04}$Ni/Al are 1.20, 1.75 and 1.54 respectively when the D and G bands in the spectra of Fig. 6 are considered. The introduction of tin clearly affects the crystallinity of the carbonaceous species formed during the reaction. These are found to be more amorphous, especially for the sample containing the lower amount of tin; which is in good accordance with the deactivation observed during the activity study. Also of interest is that for the $Sn_{0.02}$Ni/Ce-Al catalyst, two types of carbon species were found in the Raman experiments (Fig. 6). The I_D/I_G ratios of 0.83 and 2.03 indicate the presence of relatively hard carbon and softer carbonaceous species respectively.

On the other hand, the peak at 2, 960 cm^{-1} (2D-band) corresponds to graphene layers [36]. The wider this peak, the more layers of graphene exists, which culminate in graphite [37,38]. Given the absence of this in the Sn doped alumina samples, this suggests a greater amount of disorder in the graphene, confirming the beneficial effect of Sn towards hindering the formation of structured carbon.

3.6.3. TPO

TPO profiles of the spent catalysts (Fig. 7) confirm the conclusions from the Raman study. Ni/Al has a single peak at 630 °C, which backs up the Raman and SEM of predominantly only hard carbon being present, as harder carbon requires higher temperatures to oxidise [7]. Conversely, $Sn_{0.02}$Ni/Ce-Al shows 2 distinct peaks at 430 and 580 °C, confirming the presence of multiple carbon types, including some relatively crystalline and hard carbon species, as well as some less structured carbon. More importantly, for the ceria doped materials, the peaks occur at lower temperatures, corroborating the softer nature of the carbon formed on this sample in comparison to that formed over Ni/Al. Given that both peaks are similar in height, this also hints that both forms are in rather relative quantities. These results correlate fairly well with the observed activity trend in DRM; the reference material Ni/Al is the least active and displays the highest amount of carbon deposits (and a greater degree of crystallinity within these deposits). On the other hand, the catalyst promoted with Sn and CeO_2 presented superior performance in good agreement with the formation of lower concentration of carbon deposits with poorer degree of crystallinity (softer carbon).

Using the combined XRD/Raman/SEM/TPO study, the positive effects of CeO_2 and Ni regarding carbon poisoning resistance were revealed. Given the superior catalytic behaviour of the $Sn_{0.02}$Ni/Ce-Al catalysts, this sample was selected for a deeper catalytic study including the effect of operational conditions (temperature and space velocity), long term stability test, and bi-reforming reaction.

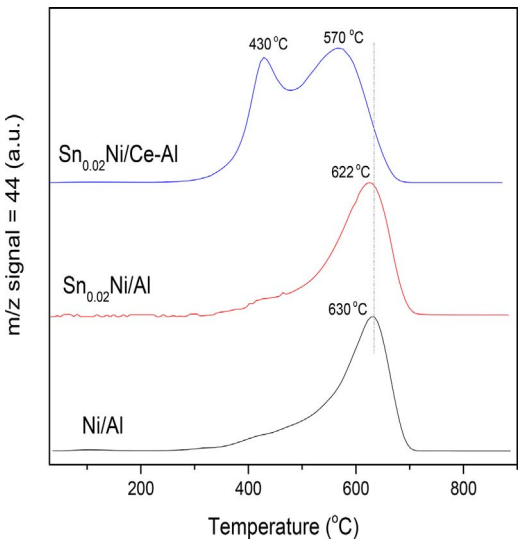

Fig. 7. TPO results conducted post DRM reaction.

3.7. Temperature effect

Given the endothermic nature of the reaction (Eq. (2)), conversions are markedly improved with an increase in temperature as shown in Fig. 8. CO_2 reaches an excellent steady conversion of 85% after 20 h at 800 °C. Methane is similarly high remaining above 40%, with both factors thereby combining to result in a stable and respectable H_2/CO ratio of 0.83.

Conversely, a lower temperature of 600 °C shows rapid deactivation from the off, with a more extreme drop off less than 4 h into experimentation. A virtually zero conversion of methane in the final stages of the reaction suggest that the active Ni has been fully cooked, due to the greater abundance of C formation at lower temperatures in fair agreement with the thermodynamic calculations (Fig. 8a). In addition, the methane conversion profile at 600 °C reflects two deactivation processes, one happening at early reaction stages and a second taking place after 4 h of reaction. This latter observation agrees perfectly with the formation of two types of carbon, a process which is thermodynamically more favoured at lower temperatures (i.e. 600 °C). A reasonably high conversion of CO_2 (35%) is still exhibited, which can likely be attributed to the RWGS (Eq. (5)) still proceeding. Further evidence of this can be confirmed by the steady H_2/CO ratio. Moreover, produced water can oxidise C to CO (Eq. (8)), which coupled with H_2 being consumed by the RWGS results in a steady ratio.

3.8. Effect of the space velocity

For both large scale and portable applications, space velocity is a key parameter which sets the volume of the reforming unit. For this test, the same gas mixture as the one described previously was used. However catalyst masses were halved and doubled (50 and 200 mg) to give WHSVs of 120,000 and 30, 000 ml/g-cat h respectively.

A higher WHSV (120,000 ml/g-cat h) means a reduced residence time, thereby not allowing sufficient time for carbon gasification to occur at the early stages, resulting in faster deactivation (Fig. 9). However after 20 h of operation, the performance to the reference 60,000 ml/g-cat h reaches similar levels. This is likely down to the surface coking reaching comparable levels, as some degree of coking is inevitable regardless of the space velocity used.

When the WHSV is decreased (30,000 ml/g-cat h), the catalyst performs significantly better at the end of the experiment, given an initially reduced activity in comparison to the reference velocity. Unlike the higher WHSV, this is inferable because the longer residence time allows time for carbon gasification to occur which diminish carbon poisoning. Also, the greater conversions can be related to the higher contact time between catalysts and reactants.

Another reason is simply down to the larger mass of catalyst used resulting in a greater concentration of active material. An increase in the number of active sites leads to both higher conversions and more sites upon which carbon can nucleate. At 30,000 ml/g-cat h this first effect outweighs the second, as reflected in the improved reactant conversions.

It should be noted that the range of space velocities selected for this work are beyond the operational space velocities for static reformers in industrial applications, which are typically around 10,000 h^{-1} [39]. This reflects an added value of these multicomponent catalysts which can operate at rather high space velocities, and consequently result in relatively smaller reactor volumes, thereby decreasing the capital cost in potential applications.

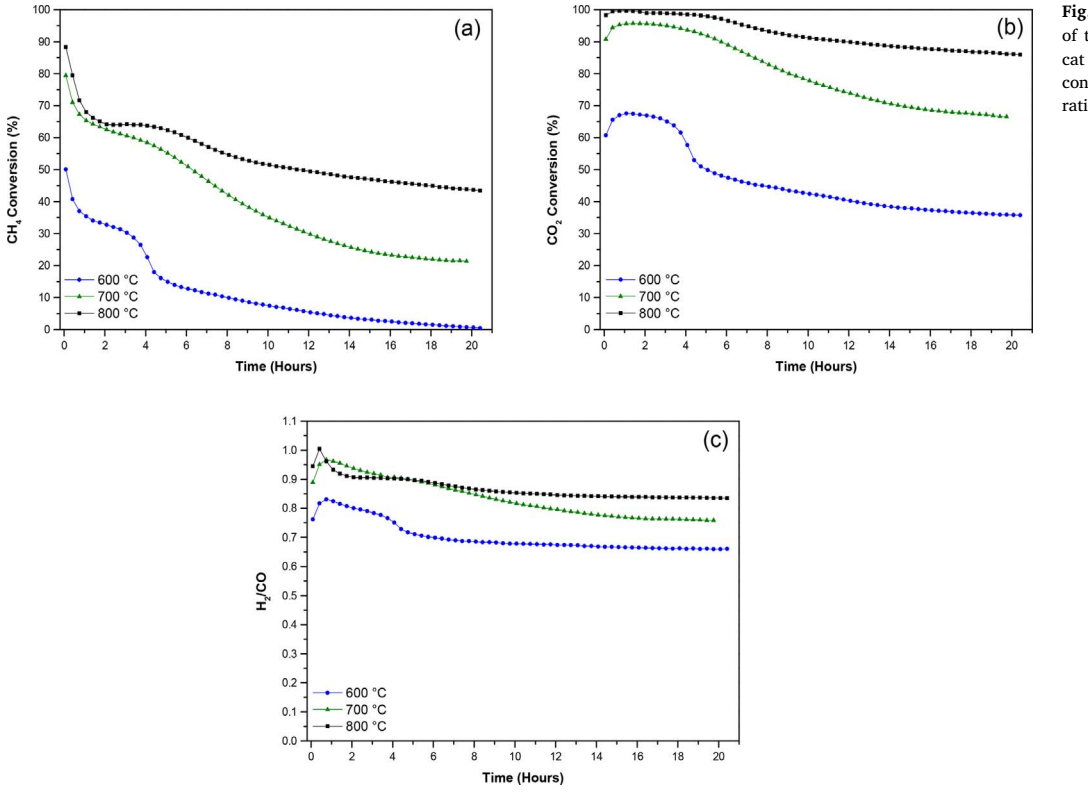

Fig. 8. DRM of $Sn_{0.02}Ni$/Ce-Al over a range of temperatures, a WHSV of 60,000 ml/(g-cat h) and a CH_4/CO_2 ratio of 1: (a) Methane conversion; (b) CO_2 conversion; (c) H_2/CO ratio.

3.9. Stability test

A long-term test lasting 92 h on the $Sn_{0.02}Ni$/Ce-Al was conducted (Fig. 10) at the same conditions used for the catalyst screening. After a rapid decline for the first 20 h (as documented during screening), the performance settles to a steady decline for the remaining 70 + hours of operation.

This equates to methane and CO_2 declination rates of approximately 0.24%/h each. The yields of CO and H_2 declined at rates of 0.21 and 0.18%/h respectively. This slight difference can be accounted to the aforementioned side reactions, and also explains why the H_2/CO ratio suffers a slight reduction over time given equal usage of both CO_2 and

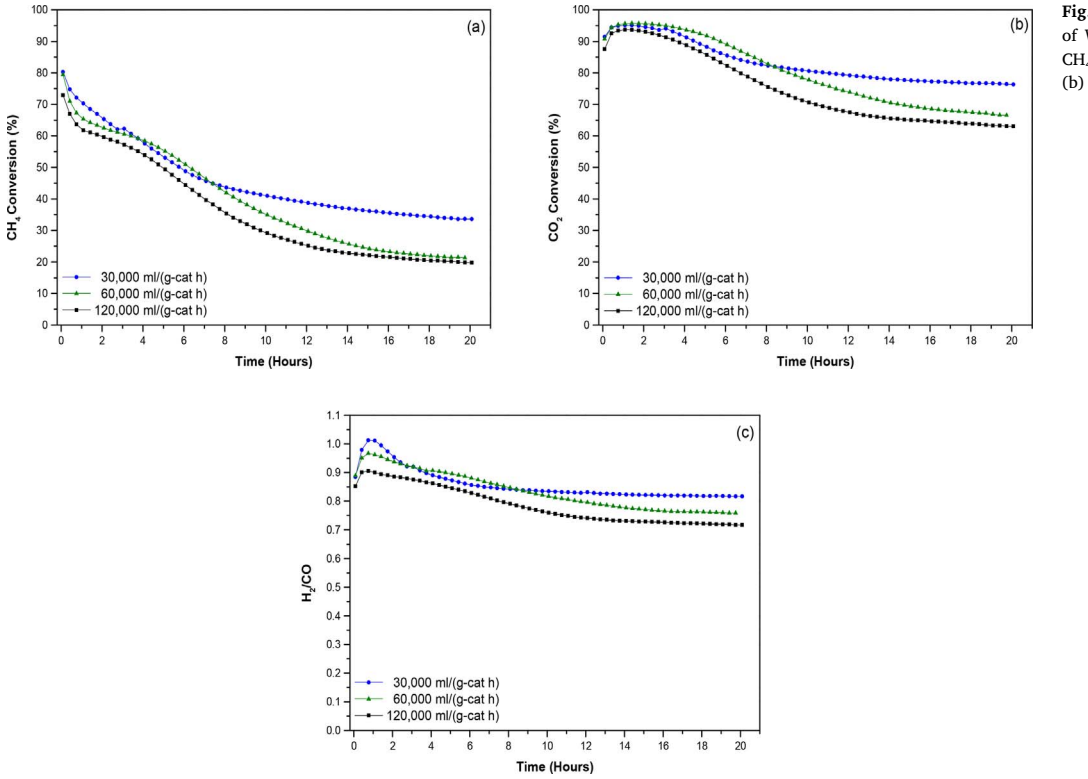

Fig. 9. DRM of $Sn_{0.02}Ni$/Ce-Al over a range of WHSVs, a temperature of 700 °C and a CH_4/CO_2 ratio of 1: (a) Methane conversion; (b) CO_2 conversion; (c) H_2/CO ratio.

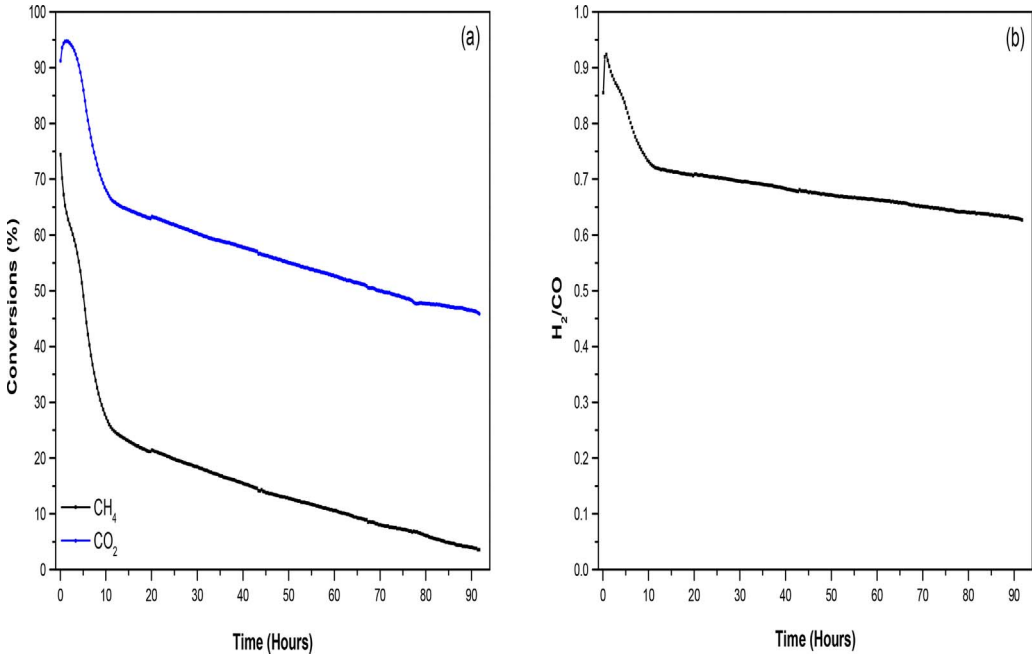

Fig. 10. DRM Stability test for $Sn_{0.02}Ni/Ce$-Al at 700 °C, WHSV of 60,000 ml/(g-cat h) and a CH_4/CO_2 of 1: (a) Methane and CO_2 conversions; (b) H_2/CO ratio.

methane.

Despite methane conversions reducing to less than 5% at the experiment conclusion, CO_2 conversion stabilised at around 70% after 20 h (in-line with the screening test), before steadily dropping to a still respectable level of just under 46% by the end. This is only marginally worse than the un-doped Ni/Al, which had a conversion of 50% after only 20 h of operation. (Fig. 5a). Therefore although the promoted catalysts perform much better than standard Ni/Al materials in DRM, there is still some room for improvements regarding the long-term stability of this multicomponent catalyst.

3.10. Bi-reforming performance

Despite the encouraging results obtained in DRM, the limitations imposed by the nature of the reaction in terms of the H_2/CO ratio motivates the bi-reforming study. Indeed when syngas is the targeted product in the chemical CO_2 upgrading, it is desirable a H_2-rich syngas (i.e. H_2/CO = 1.5–2) which makes it more versatile for several applications, including methanol production or Fischer-Tropsch synthesis. In the BRM runs, reaction conditions were kept as similar as possible to DRM for ease of comparison of results for $Sn_{0.02}Ni/Ce$-Al (Fig. 11).

As shown in Fig. 11c, the H_2/CO ratio remains above 1.6 for the duration of the test, which sits on the equilibrium line (as predicted by the previously described thermodynamics). This is an excellent result indicating that this catalyst can produce a relatively high quality syngas by introducing some water in the reforming mixture. Whereas the utilisation of $Sn_{0.02}Ni/Ce$-Al in DRM never leads to the maximum allowed H_2/CO ratio, the addition of water changes the scenario underlining the suitability of this material for BRM.

Similarly, a much higher conversion of methane is exhibited, remaining at a constant level of 70% for the duration of the experiment. This remarkable stability has not been exhibited for any of the DRM reactions; regardless of the catalyst or conditions used. Having such a stable conversion is doubly impressive given that the primary means for carbon deposition is via the disassociation of methane. The improvement on methane conversion can be attributed to the presence of steam reforming as a parallel reaction, which also helps to boost the hydrogen yield. Also, the more stable trends indicate less deactivation in comparison with DRM. In fact for the dry reforming of methane, both reactants are potential sources of carbon, making the development of stable catalysts more challenging. In contrast, the introduction of water in the bi-reforming reaction alleviates the amount of potential coking molecules, and aids also the gasification of carbonaceous species attached to the catalyst surface.

All the inherent features of the bi-reforming are boosted by the presence of a carefully designed catalyst, such as the one presented in this study. The active phase (Ni) has been promoted with a group IV element (Sn), the valance shell of which is isoelectronic to C and can occupy the C nucleation positions, thus coking is mitigated. Yet more, the presence of ceria in the catalyst formulation enhances Ni dispersion. Ceria is a highly defective material, where oxygen vacancies are considered preferential sites for metallic particles to deposit, helping to achieve high metallic dispersion [40]. The greater dispersion of Ni in the presence of ceria benefits the catalytic performance. On top of this, oxygen vacancies in ceria also play a role in carbon tolerance. These partially avoid carbon deposition or simply help to form softer carbon species, as demonstrated by Raman and TPO experimentation.

A lower conversion of CO_2 is noted, as predicted by the thermodynamics. This is primarily driven by the WGS (Eq. (5)), as the water in the feed drives the formation of CO_2, reducing the overall conversion. Herein, CeO_2 is an active catalyst for the shift reaction [41], and therefore the presence of the WGS becomes more visible for BRM. However the conversion is still valuable, and remains mostly stable at 40% over the course of the experiment.

Roh et al. [42] similarly found this level of stability for Ni-Ce catalysts towards BRM. This factor was accredited to the high surface area and dispersion of the Ni, as well as the OSC of CeO_2. A high dispersion of $Sn_{0.02}Ni/Ce$-Al was noted by the SEM imagery, but the surface area saw a decrease (Table 1), thus suggesting Ni dispersion is of greater importance.

Another benefit of BRM is the fact that longer chained hydrocarbons can also be converted in the presence of steam and CO_2 [3]:

$$3C_nH_{2n+2} + (3n\text{-}1)H_2O + CO_2 \rightarrow (3n + 1)CO + (6n + 2)H_2 \quad (15)$$

This allows a flexibility in the fuel source as shale gas and biogas, for example, are predominantly composed of methane, they also contain larger chains [43]. Therefore by showing a favourable stability for BRM, it can be hypothesised $Sn_{0.02}Ni/Ce$-Al will perform well with a feed mixed of various hydrocarbons.

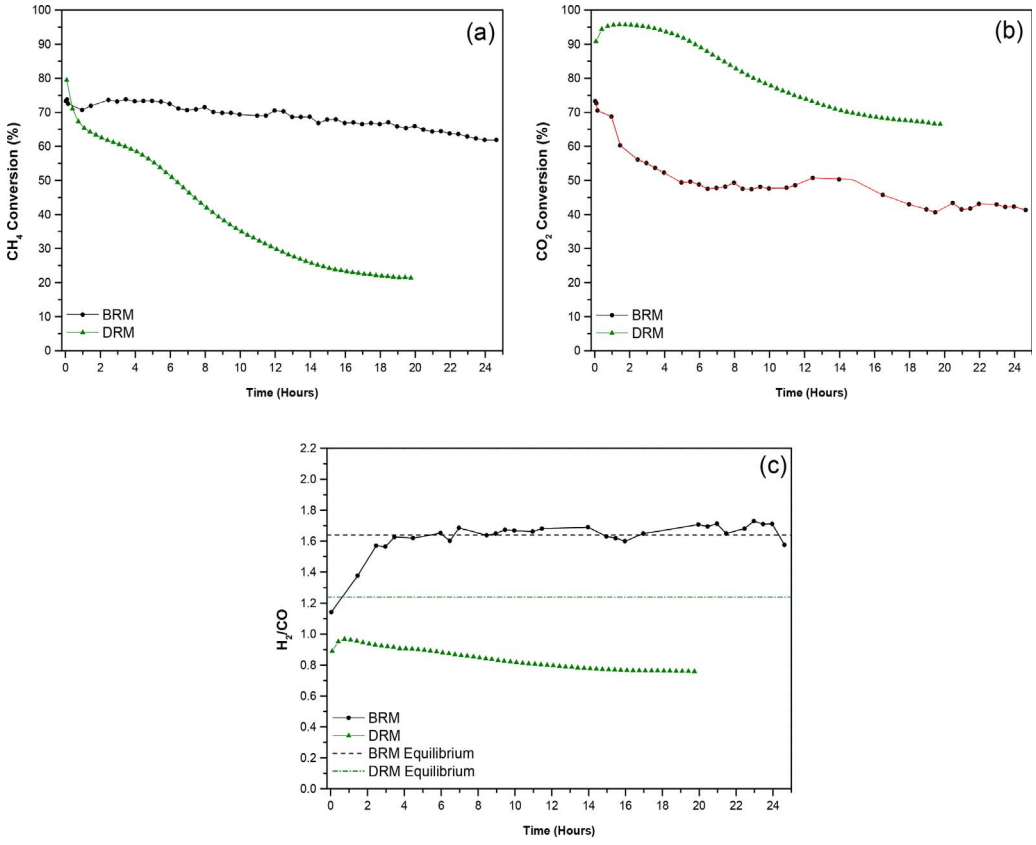

Fig. 11. Comparison of DRM (CH_4/CO_2 = 1) and BRM (CH_4/CO_2/H_2O = 1/1/1) for $Sn_{0.02}$Ni/Ce-Al at 700 °C and WHSV of 60, 000 ml/(g-cat h): (a) Methane conversion; (b) CO_2 conversion; (c) H_2/CO ratio.

4. Conclusions

A new series of multicomponent advanced catalysts for chemical CO_2 recycling in the gas phase has been developed in this work. The catalytic design is tailored using a reference Ni/Al_2O_3 catalyst and promoting this standard material with Sn and CeO_2. Through the addition of small quantities of these dopants, the performance towards dry reforming of methane can be improved. This extends to conversions of both CO_2 and methane, as well as producing a good H_2/CO ratio. The positive effect of tin is credited to Sn atoms occupying C nucleation sites in the vicinity on Ni atoms, slowing coke formation mechanisms in the process. However, a large amount of Sn can have a detrimental effect on the performance by covering Ni active sites, restricting the access of reactants and thereby reducing conversions. Consequently, this makes it necessary to find a suitable trade-off between activity and stability, where the optimum amount has been identified at a Sn/Ni molar ratio of 0.02.

Moreover, further improvement towards carbon deposition was achieved by introducing CeO_2. When ceria is present, the high oxygen storage capacity and the modified acid/base properties of the support lead to an enhanced performance. Indeed, the multicomponent catalyst $Sn_{0.02}$Ni/Ce-Al performs well over a range of temperatures and space velocities. It has also proven to remain active for a long period (92 h). This catalyst was then tested for the bi-reforming of methane reaction using comparable conditions to DRM. A remarkable level of stability and excellent conversions were noted, proving the versatility of this catalyst to upgrade a variety of CO_2 containing feedstocks. Certainly, a high quality syngas was obtained in the bi-reforming experiments with our advanced catalysts.

Overall, this work provides a strategy for designing highly efficient and economic catalysts for flexible syngas production from CO_2/CH_4 mixtures. This therefore paves the way for potential applications in technologies addressing the global challenge of CO_2 emissions.

Acknowledgments

Financial support for this work was provided by the Department of Chemical and Process Engineering at the University of Surrey and the EPSRC grant EP/R512904/1. E. Le Sache acknowledges the Erasmus+ programme for her fellowship which allowed her to conduct part of the experiments in Spain. The Spanish team acknowledges the financial support obtained from the Spanish Ministry of Economy and Competitiveness (ENE2015-66975-C3-2-R) and from Junta de Andalucía (TEP-8196), both co-financed by FEDER funds from the European Union.

References

[1] J.C.M. Pires, F.G. Martins, M.C.M. Alvim-Ferraz, M. Simoes, Chem. Eng. Res. Des. 89 (2011) 1446–1460.
[2] A. Taheri Najafabadi, Int. J. Energy Res. 37 (2013) 485–499.
[3] N. Kumar, M. Shojaee, J.J. Spivey, Curr. Opin. Chem. Eng. 9 (2015) 8–15.
[4] I.H. Son, S.J. Lee, A. Soon, H.S. Roh, H. Lee, Appl. Catal. B: Environ. 134–135 (2013) 103–109.
[5] H.S. Roh, K.Y. Koo, J.H. Jeong, Y.T. Seo, D.J. Seo, Y.S. Seo, W.L. Yoon, S. Bin Park, Catal. Lett. 117 (2007) 85–90.
[6] V.R. Choudhary, A.M. Rajput, Rajput Choudhary, Ind. Eng. Chem. Res. 35 (1996) 3934–3939.
[7] D. Pakhare, J. Spivey, Chem. Soc. Rev. 43 (2014) 7813–7837.
[8] N.D. Charisiou, G. Siakavelas, K.N. Papageridis, A. Baklavaridis, L. Tzounis, D.G. Avraam, M.A. Goula, J. Nat. Gas Sci. Eng. 31 (2016) 164–183.
[9] S.S. Itkulova, G.D. Zakumbaeva, Y.Y. Nurmakanov, A.A. Mukazhanova, A.K. Yermaganbetova, Catal. Today 228 (2014) 194–198.
[10] P. Boldrin, E. Ruiz-Trejo, J. Mermelstein, J.M. Bermúdez Menéndez, T. Ramírez Reina, N.P. Brandon, Chem. Rev. 116 (2016) 13633–13684.
[11] M.M. Danilova, Z.A. Fedorova, V.A. Kuzmin, V.I. Zaikovskii, A.V. Porsin, T. Krieger, Catal. Sci. Technol. 5 (2015) 2761–2768.
[12] O.A. Bereketidou, M.A. Goula, Catal. Today 195 (2012) 93–100.
[13] M.-S. Fan, A.Z. Abdullah, S. Bhatia, ChemCatChem 1 (2009) 192–208.
[14] P. Djinović, J. Batista, A. Pintar, Int. J. Hydrogen Energy 37 (2012) 2699–2707.
[15] A. Vita, L. Pino, F. Cipitì, M. Laganà, V. Recupero, Fuel Process. Technol. 127 (2014).
[16] S. Wang, G.Q. Lu, Appl. Catal. B: Environ. 19 (1998) 267–277.
[17] H. Wu, V. La Parola, G. Pantaleo, F. Puleo, A. Venezia, L. Liotta, Catalysts 3 (2013)

563–583.
[18] L. Pastor-Pérez, A. Merlo, R. Buitrago-Sierra, M. Casella, A. Sepúlveda-Escribano, J. Colloid Interface Sci. 459 (2015) 160–166.
[19] L. Pastor-Pérez, A. Sepúlveda-Escribano, Fuel 194 (2017) 222–228.
[20] L. Pastor-Pérrez, A. Sepúlveda-Escribano, Appl. Catal. A: Gen. 529 (2017) 118–126.
[21] S.A. D'Ippolito, C.R. Vera, F. Epron, P. Samoila, C. Especel, P. Marécot, L.B. Gutierrez, C.L. Pieck, Appl. Catal. A: Gen. 370 (2009) 34–41.
[22] J. Bussi, M. Musso, A. Quevedo, R. Faccio, M. Romero, Catal. Today 296 (2017) 154–162.
[23] D. Baudouin, J.P. Candy, U. Rodemerck, F. Krumeich, L. Veyre, P.B. Webb, C. Thieuleux, C. Copéret, Catal. Today 235 (2014) 237–244.
[24] V.G. Deshmane, S.L. Owen, R.Y. Abrokwah, D. Kuila, J. Mol. Catal. A: Chem. 408 (2015) 202–213.
[25] S.M. de Lima, A.M. da Silva, G. Jacobs, B.H. Davis, L.V. Mattos, F.B. Noronha, Appl. Catal. B: Environ. 96 (2010) 387–398.
[26] D. Trimm, Catal. Today 49 (1999) 3–10.
[27] Z. Hou, O. Yokota, T. Tanaka, T. Yashima, Appl. Surf. Sci. 233 (2004) 58–68.
[28] A. Penkova, L. Bobadilla, S. Ivanova, M.I. Domínguez, F. Romero-Sarria, A.C. Roger, M.A. Centeno, J.A. Odriozola, Appl. Catal. A: Gen. 392 (2011) 184–191.
[29] G.G. Kuvshinov, Y.I. Mogilnykh, D.G. Kuvshinov, V.I. Zaikovskii, L.B. Avdeeva, Carbon N. Y. 36 (1998) 87–97.
[30] R.T.K. Baker, M.A. Barber, P.S. Harris, F.S. Feates, R.J. Waite, J. Catal. 26 (1972) 51–62.
[31] R.T.K. Baker, P.S. Harris, R.B. Thomas, R.J. Waite, J. Catal. 30 (1973) 86–95.
[32] J. Wei, E. Iglesia, J. Catal. 224 (2004) 370–383.
[33] M. Kovacevic, B.L. Mojet, J.G. Van Ommen, L. Lefferts, Catal. Lett. 146 (2016) 770–777.
[34] J.W. Shabaker, G.W. Huber, J.A. Dumesic, J. Catal. 222 (2004) 180–191.
[35] L. Tzounis, M. Kirsten, F. Simon, E. Mäder, M. Stamm, Carbon N. Y. 73 (2014) 310–324.
[36] A.C. Ferrari, Raman Spectrosc. Graphene Graphite: Solid State Commun. 143 (2007) 47–57.
[37] A.C. Ferrari, J.C. Meyer, V. Scardaci, C. Casiraghi, M. Lazzeri, F. Mauri, S. Piscanec, D. Jiang, K.S. Novoselov, S. Roth, A.K. Geim, Phys. Rev. Lett. 97 (2006) 1–4.
[38] R. Saito, M. Hofmann, G. Dresselhaus, A. Jorio, M.S. Dresselhaus, Adv. Phys. 60 (2011) 413–550.
[39] J.-M. Lavoie, Front. Chem. 2 (2014) 1–17.
[40] T.R. Reina, S. Ivanova, O.H. Laguna, M.A. Centeno, J.A. Odriozola, Appl. Catal. B: Environ. 197 (2016) 67–72.
[41] T.R. Reina, S. Ivanova, M.A. Centeno, J.A. Odriozola, Int. J. Hydrogen Energy 40 (2015) 1782–1788.
[42] H.S. Roh, K.Y. Koo, W.L. Yoon, Catal. Today 146 (2009) 71–75.
[43] G.A. Olah, A. Goeppert, M. Czaun, G.K.S. Prakash, J. Am. Chem. Soc. 135 (2013) 648–650.